# Monte Carlo Phase Diagram of Symmetric Diblock Copolymer in Selective Solvent

**S. Wołoszczuk,[†] M. Banaszak,*[,†] P. Knychała,[†] and M. Radosz[‡]**

*Institute of Physics, A. Mickiewicz University, ul. Umultowska 85, 61-614 Poznan, Poland, and Soft Materials Laboratory, Department of Chemical and Petroleum Engineering, University of Wyoming, Laramie, Wyoming 82071-3295*

*Received August 14, 2007; Revised Manuscript Received June 9, 2008*

ABSTRACT: With a lattice Monte Carlo method, we investigate 16−16 symmetric diblock in selective solvent, A-*b*-B/A, at 10 volume fractions from 1.0 to 0.1, and for each volume fraction, we perform simulations at up to 54 temperatures, using simulation boxes of different sizes. We report temperature dependencies for a number of quantities such as energy, specific heat, and mean-squared end-to-end distances and construct a phase diagram using the thermodynamic and structural quantities as well as snapshots of the selected configurations. The simulated phase diagram is compared with the experimental data of Lodge and co-workers for nearly symmetric poly(styrene-*b*-isoprene) mixed with dimethyl phthalate.

## I. Introduction

Phase behavior of diblock copolymer solutions is of great relevance for a plethora of reasons, both academic and practical.[1−5] Depending on the amount of solvent, different concentration regimes can be obtained, ranging from pure copolymer melt to a dilute copolymer solution, and also two distinct intermediate concentration regimes referred to as concentrated and semidilute.[1] At high concentrations the copolymer solutions are considerably similar to pure diblock copolymer melts which are known to self-assemble into a variety of ordered nanostructures, also referred to as microphases (or phases for short), via the microphase separation transition (MST) which is an instance of the order−disorder transition (ODT). For equilibrated neat diblock copolymer melts, these nanostructures include ordered layers (L), ordered cylinders (C), ordered gyroid phase (G), and ordered spheres (S).[6] The nanostructure can be predicted from theory if temperature (or the Flory interaction $\chi$ parameter), composition, $f$, and the degree of polymerization, $N$, are known. But in the mean-field theories, it is sufficient to know the composition, $f$, and the product $N\chi$ in order to foresee the phase.[5,7]

Adding selective solvent tends to dissolve the nanostructure if the system is close to the ODT temperature. Moreover, in addition to possible microphase separation, there is a likelihood of macrophase separation, that is, a separation on a macroscopic scale into two phases, as known from experiment and also predicted by theory. Therefore, the phase behavior of symmetric A-*b*-B/A solution is largely determined by a competition between microphase and macrophase separations. While for the system considered, all single-phase regions are separated by two-phase regions; there is a good reason to expect these two-phase regions to be very narrow. Both experiment[8] and the self-consistent-field theory (SCFT) for copolymer/(short homopolymer)[9] point to this possibility at simulated state points. In this work, therefore, we do not take into account the possibility of the macrophase separation. At very low concentrations, below the critical micelle concentration (CMC), spatially disordered micelles are formed. This rather complex phase behavior of the A-*b*-B/A solution has been studied experimentally, e.g, ref 8, and theoretically, e.g. ref 10. There are, however, no computer-simulated phase diagrams of such solutions. Computer simulations of self-assembling copolymer systems pose a considerable challenge because of the finite size effects,[11] and the addition of solvent introduces a further complexity. As far as static properties are concerned, the Monte Carlo methods tend to be more efficient than the molecular dynamics (MD) methods because they allow faster probing of the phase space. Lattice models are more efficient than continuum models. They capture essential physics of polymer solutions in the spirit of the mean-field Flory−Huggins approach, which works particularly well for the melts and concentrated solutions. Recently, Matsen and co-workers have successfully applied a lattice Monte Carlo method to construct a phase diagram for the diblock melt.[12,13]

The goal of this study is to determine a phase diagram of symmetric A-*b*-B/A solutions using a lattice Monte Carlo method with cooperative motion algorithm (CMA)[14,15] developed by Pakula and co-workers, as presented in ref 16. Such a CMA model of lattice liquid, in contrast to lattice gas, does not require any vacancies to perform the rearrangements, and hence it is ideally suited for dense polymeric systems. For the sake of consistency, however, we want to use it at all copolymer volume fractions, but to compare CMA results with a simple Monte Carlo method (that is, without cooperative moves) at very low volume fractions (for which CMA is less efficient) to verify that both approaches yield the same data.

## II. Model and Simulation

The simulations are performed using CMA for a face-centered cubic (FCC) lattice with the coordination number $z = 12$ and the bond length $\sqrt{2}a$, where $a$ is the FCC lattice constant. Chain bonds are not allowed to be broken or stretched, and the usual periodic boundary conditions are imposed. The lattice box size is chosen to fit the chain, and the lattice sites are completely filled with chain segments and solvent segments; there are no vacancies. Since all lattice sites are occupied, a chain segment or a solvent segment can move if other segments move simultaneously. An attempt to move a single segment defines a single Monte Carlo step. A 16−16 A-*b*-B copolymer block consists of 16 segments each. The solvent is of type A; it interacts in a different way with A-block (it is always a "good" solvent for the A-block) and in a different way with the B-block (solvent quality for the B-block varies with temperature), which means that it is selective. The interaction energy between segments of types $i$ and $j$ is given by $\epsilon_{ij}$, where $\epsilon_{AA} = 0$, $\epsilon_{AB} =$

* Corresponding author. E-mail: mbanasz@amu.edu.pl.
[†] A. Mickiewicz University.
[‡] University of Wyoming.

10.1021/ma0718346 CCC: $40.75 
Published on Web 07/16/2008

$\epsilon$, $\epsilon_{BB} = 0$, $\epsilon_{AS} = 0$, $\epsilon_{BS} = \epsilon$, $\epsilon_{SS} = 0$; A and B denote the chain segments, and S denotes the solvent segment. The interaction is limited to the nearest neighbors ($z = 12$), and the interaction parameter, $\epsilon$, is related to the Flory $\chi$ parameter by the following equation:

$$\chi = \frac{(z-2)\epsilon}{kT} \tag{1}$$

This parameter, $\epsilon$, serves also as an energy unit to define the reduced energy per lattice site and the reduced temperature as

$$\frac{E^*}{n_a} = \frac{E/\epsilon}{n_a} \tag{2}$$

$$T^* = \frac{kT}{\epsilon} \tag{3}$$

where $n_a$ is the number of lattice sites.

First, we choose the 32 × 32 × 32 FCC box (with $n_a = 2^{15}/2 = 2^{14} = 16\,384$ sites) in order to fit a fully extended 16−16 copolymer chain. The FCC lattice is generated from a simple cubic 32 × 32 × 32 lattice by removing every second site (to satisfy the condition that the sum of integer coordinates, $x + y + z$, is an odd integer). For the copolymer melt, the whole FCC lattice is filled with copolymer chains, which means that there are $n_a/N = 2^9 = 512$ chains ($N = 32$ is the total number of segments in the diblock chain). In this work, we simulate 10 different copolymer volume fractions, $\Phi$, starting with a copolymer melt, $\Phi = 1.0$, followed by a series of copolymer solutions, $\Phi = 460/512 \approx 0.9$, $410/512 \approx 0.8$, $358/512 \approx 0.7$, $308/512 \approx 0.6$, $256/512 = 0.5$, $205/512 \approx 0.4$, $154/512 \approx 0.3$, $102/512 \approx 0.2$, and $51/512 \approx 0.1$. For a volume fraction of 0.9 (460/512 to be exact), we have 460 diblock chains and 1664 solvent segments; the solvent segments can be thought of as replacing the 52 (512−460) melt diblock chains ($52N = 1664$). In a similar manner, the number of chains and segments can be calculated for the remaining volume fractions, from $\Phi = 0.8$ to $\Phi = 0.1$. We investigate the size effects by performing simulations in boxes of various sizes. In particular, we carry out systematic studies for the 64 × 32 × 32 and the 64 × 64 × 64 FCC simulation boxes, with the number of copolymer chains greater 4 and 8 times, respectively, than the number of chains for the initial box (32 × 32 × 32) at a given volume fraction. For each volume fraction, $\Phi$, we perform a series of simulations for at least 24 (up to 54) different temperatures, $T^*$, for the smallest box, and for larger boxes, we simulate at selected temperatures of interest.

First, we equilibrate the system in the athermal limit, that is, where $\epsilon/(kT)$ is zero. When the system reaches its thermal equilibrium, the polymer chains assume statistical conformations, random orientations, and become uniformly distributed within the simulation box. We record the translational diffusion of the copolymer chains in order to estimate the simulation time scale. In the athermal melt, it takes about $1.4 \times 10^4$ MC timesteps to diffuse at a distance of the order of the radius of gyration of the 16−16 copolymer chain; this time is shorter for the copolymer solutions. We equilibrate the athermal melt and the copolymer solutions for $2 \times 10^7$ MC timesteps. From the equilibrated melt state, the system is quenched to a required temperature. This procedure is fully described in ref 17. We perform at least $6 \times 10^6$ Monte Carlo (MC) timesteps above $T^* = 2.5$ and at least $10 \times 10^6$ MC timesteps (up to $60 \times 10^6$) below $T^* = 2.5$. For a given $T^*$ and $\Phi$ we repeat the simulation experiment at least four times starting with different initial states. For a given state point, all runs yield the same type of nanostructure, and the results are averaged over all such runs. We also verify the quality of thermal equilibration, by heating the system up and then cooling it down again. Usually, we also assume that the first half of run is needed to equilibrate the system, and the second half is used to collect the data.

## III. Results and Discussion

The phase diagrams of the A-*b*-B/A solution, shown in Figure 1, summarize the scope of the work presented in this paper for simulation boxes of different sizes (a, b, and c). Figure 1d shows the final phase diagram for all three simulation boxes, 32 × 32 × 32, 64 × 32 × 32, and 64 × 64 × 64. Different nanostructures are shown as a function of the copolymer volume fraction, $\Phi$, and temperature, $T^*$. At high $T^*$, that is above $T^* = 16$ for $\Phi = 1$ and above 6 for 0.1, a disordered phase is observed, which confirms that increasing solvent concentration inhibits the nanostructure formation. In this work, we observe five nanostructures (L, B, PL, C, and S), including the three phases L, C, and S referred to in the Introduction. We also observe a bicontinuous phase (B), which is very similar to gyroid phase (G). We call it "bicontinuous" because it is difficult to confirm a full space group symmetry ($Ia\bar{3}d$) of the simulated configurations. For neat diblock melts, the G phase known to be stable in a narrow volume windows between layers and cylinders has a bicontinuous cubic structure, in which the minority component microdomains form interweaving left-hand and right-hand 3-fold-coordinated lattices. In addition, we observe a perforated lamellar phase (PL) which is known to be metastable for neat diblock melts. However, its stability for diblock solutions remains an open question. In general, in Figure 1 the thick line indicates ODT, whereas the shaded dotted lines indicate order−order transitions (OOT). These lines are not very accurate because there are data only for 10 copolymer volume fractions (denoted with filled circles for the ODT lines and open circles for the OOT lines). The data above $T^* = 2$ are the same for all volume fractions, irrespective of the box size, except for $\Phi = 0.7$. For this volume fraction, where either phase B or PL is observed, the cubic B phase is promoted by the cubic symmetry of the 32 × 32 × 32 and 64 × 64 × 64 boxes. In the 64 × 32 × 32 simulation box, for which the cubic symmetry is broken, we observe only PL phase at $\Phi = 0.7$ for all temperatures below the ODT line. In Figure 1d, which is meant to summarize the data, the symbol BPL means B or PL phase. The phase diagram presented in Figure 1d is *similar* to the experimental phase diagram of Lodge and co-workers[8] for poly(styrene-*b*-isoprene) (SI) with similar blocks (15−13) mixed with dimethyl phthalate (DMP), as shown in Figure 2.

The simulation method, which we use, is not suitable for calculating binodals for the copolymer/solvent macrophase separation. The free energy needed to estimate binodals for such copolymer/solvent system can be calculated, for example, using SCFT.[5,10] While we do not perform such calculations in this study, it is known, for example from Matsen's work[9] and Lodge's experiment,[8] that all single-phase regions are separated by two-phase regions. However, there is a good reason to expect these two-phase regions are very narrow for the simulated state points. In this work, therefore, we do not take into account the possibility of the macrophase separation.

The nanostructures identified by examining the MC configurations at all temperatures, volume fractions, and box sizes are illustrated by representative snapshots shown in Figures 3–6. We also report the total energy, $E^*/n_a$, the specific heat, $C_v$, the total end-to-end distance, $R^2$, and the end-to-end distances for individual blocks, $R_A^2$ and $R_B^2$ shown in Figures 7–9. For example, for pure melt ($\Phi = 1$) shown in Figure 3, we report a lamellar phase below $T^* = 16$ (that is, above $\chi N = 20$). The classical mean-field result for a symmetric diblock melt is $\chi_c N = 10.5$[7] (where $\chi_c$ is the critical value of the Flory interaction parameter), but it is well-known that the inclusion of fluctuations will shift this value significantly for relatively short chains.[18]

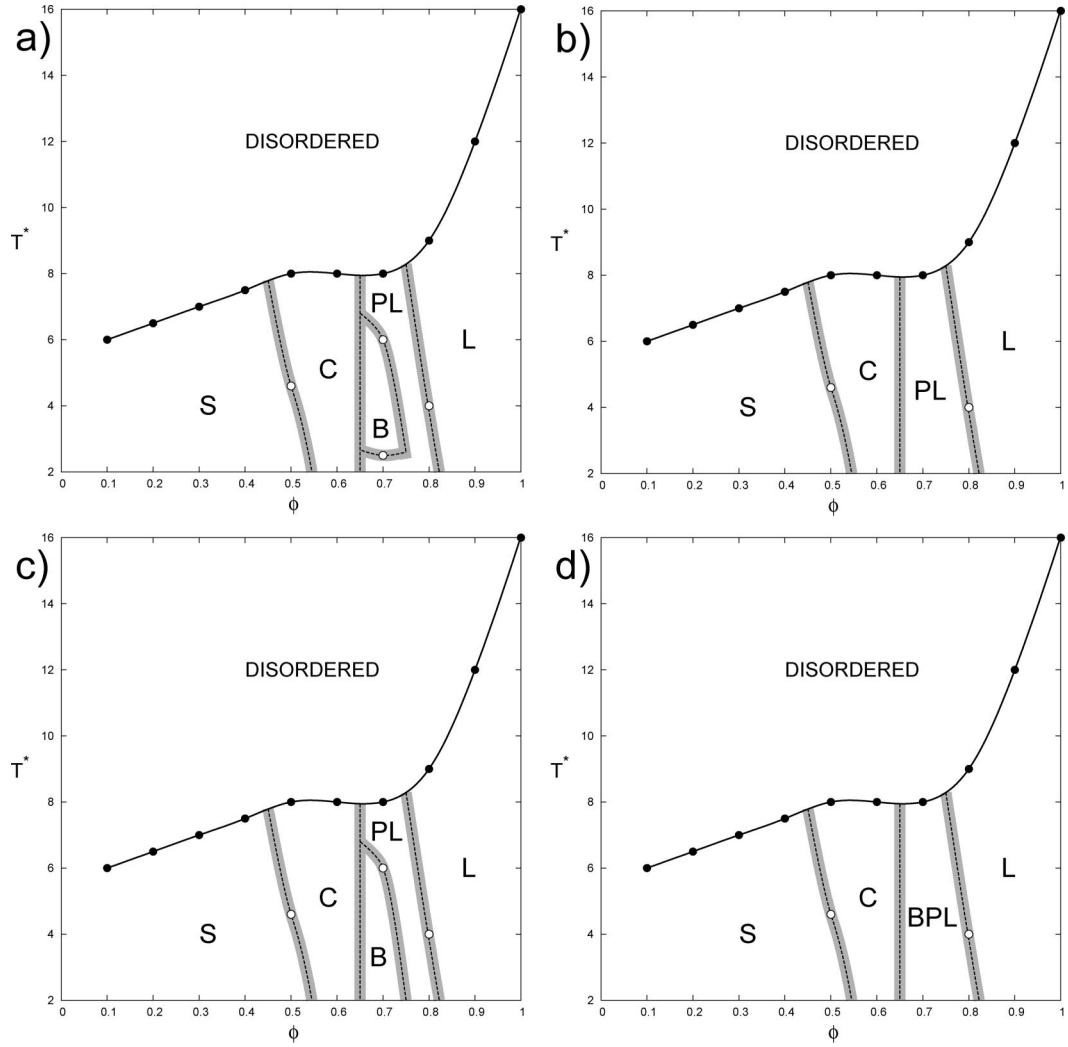


**Figure 1.** Phase diagrams of 16−16 symmetric diblock in selective solvent, A-*b*-B/A, as a function of $T^*$ and $\Phi$, where L indicates lamellar phase, B a bicontinuous phase, C cylindrical phase, S spherical phase, and PL perforated lamellar phase; solid line is the approximate ODT line, and the shaded dotted lines are the approximate OOT lines. (a) Results for the 32 × 32 × 32 simulation box, (b) results for the 64 × 32 × 32 simulation box, (c) results for the 64 × 64 × 64 simulation box, and (d) phase diagram from all simulated sizes. BPL denotes a approximate phase region where either B or PL phase is reported depending on the box size.

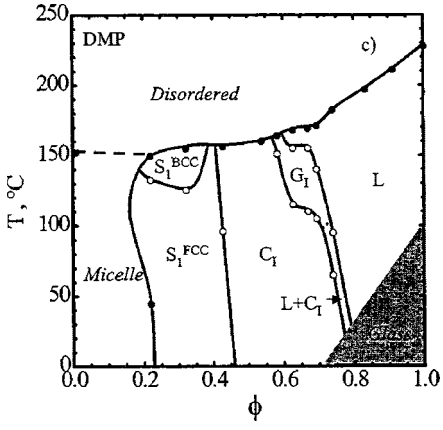


**Figure 2.** Experimental phase diagram of poly(styrene-*b*-isoprene) (SI) with similar blocks[15,13] mixed with the DMP, obtained by Lodge and co-workers.[8]

For a concentrated solution at $\Phi = 0.9$, we observe a lamellar phase at all temperatures below $T^*_{ODT} = 12.0$, whereas at $\Phi = 0.8$ we observe a lamellar phase below $T^*_{ODT} = 9.0$ and a PL phase below $T^* = 4.0$. For $\Phi = 1.0$, 0.9, and 0.8, both the ODT temperatures and the OOT temperature do not depend on the box size. Moreover, we do not show the phase data below $T^* = 2.0$ because such data are uncertain, as explained later for the low-temperature simulations, and they are not crucial to the main conclusion of this work.

At $\Phi = 0.7$, we report phases B (Figure 4) and PL (Figure 5), with the phase boundaries seemingly depending on the box symmetry. This copolymer volume fraction corresponds to 0.35 volume fraction of minority (B) segments, and the neat copolymer melt with $f_B = 0.35$ composition self-assembles into gyroid phase under proper state conditions.[19] For the 32 × 32 × 32 box, the B phase is observed from $T^* = 2.2$ to $T^* = 6.0$, and the PL phase is observed from $T^* = 6.0$ to $T^*_{ODT} = 8.0$ and below $T^* = 2.2$. For the 64 × 32 × 32 box, the PL phase is reported for all $T^*$'s below the ODT temperature, and for the 64 × 64 × 64 box, the PL phase is observed above $T^* = 6.0$ and the B phase below $T^* = 6.0$. In summary, for the cubic boxes (32 × 32 × 32 and 64 × 64 × 64), we observe the B phase below $T^* = 6.0$, whereas for the box with broken cubic symmetry (64 × 32 × 32), only the PL phase is observed. For the smaller box, the PL phase is cubically perforated (Figure 5a; probably an artifact of a small size of the box), whereas for the larger box, the PL phase is hexagonally perforated, which is similar to the experiments that revealed metastable hexagonally perforated lamellar phase. It is known for neat diblock

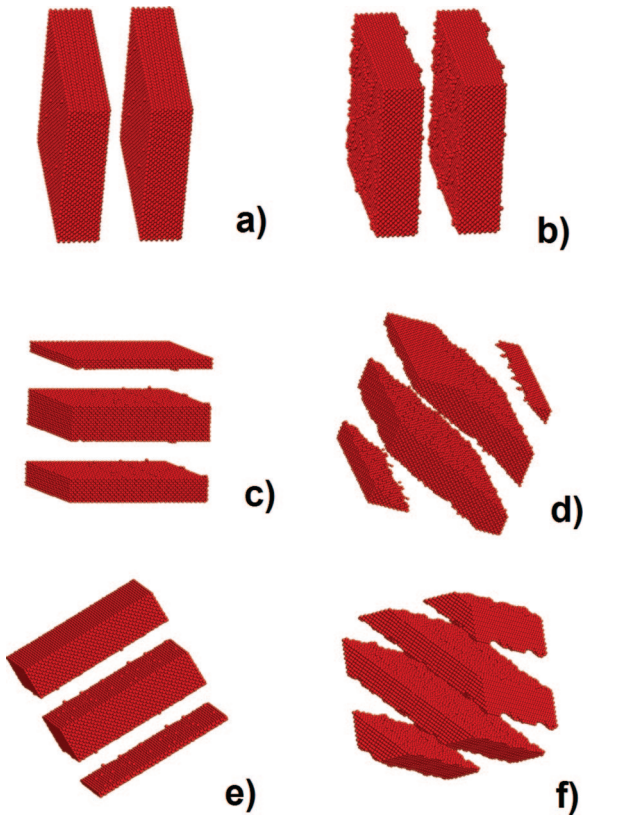


**Figure 3.** Snapshots of lamellar phase at $\Phi = 1.0$; only B-blocks are shown. The interface between lamellar microdomains is diffused at higher $T^*$'s (right-hand side) and sharp at lower $T^*$'s (left-hand side). (a) The $32 \times 32 \times 32$ box at $T^* = 0.6$; (b) the $32 \times 32 \times 32$ box at $T^* = 1.5$; (c) the $64 \times 32 \times 32$ box at $T^* = 1.0$; (d) the $64 \times 32 \times 32$ box at $T^* = 3.0$; (e) the $64 \times 64 \times 64$ box at $T^* = 1.0$; and (f) the $64 \times 64 \times 64$ box at $T^* = 3.0$.

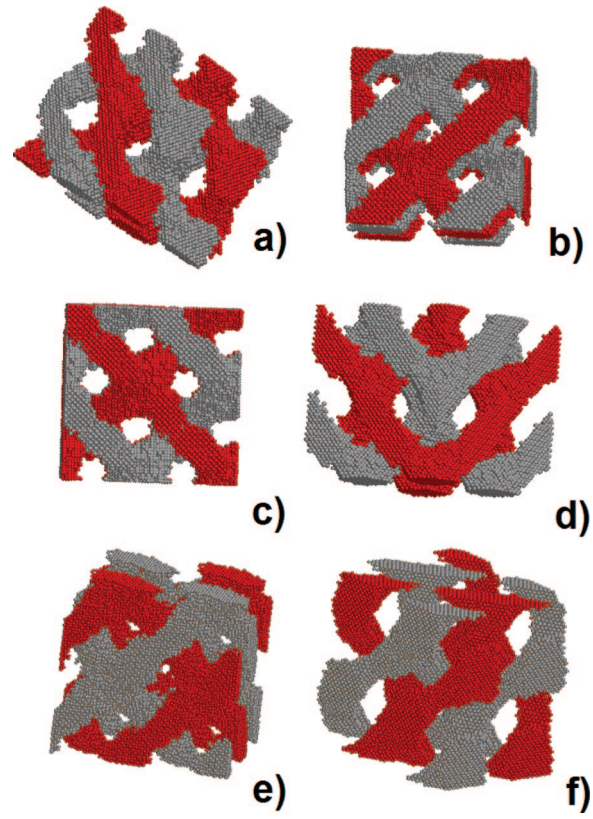


**Figure 4.** Snapshots of bicontinuous phase at $\Phi = 0.7$; only B-blocks are shown. There are two continuous interweaving components of B segments; one is shown in darker color and the other in lighter color. (a–d) The $32 \times 32 \times 32$ box at $T^* = 4.0$; (e) the $64 \times 64 \times 64$ box at $T^* = 3.7$; and (f) the $64 \times 64 \times 64$ box at $T^* = 4.3$.

melts (but not for diblock solutions) that the PL phase is metastable, and it is observed in the same phase diagram region as the stable gyroid phase. It is possible that also for copolymer solutions the PL phase is metastable, covering the stable G phase, and the B phase might also correspond to the G phase. If this is the case, the BPL phase in Figure 1d will correspond to the G phase. At lower volume fractions, say $\Phi = 0.6$, we observe the C phase for all temperatures below $T_{ODT} = 8.0$ and for all box sizes. For $\Phi = 0.5$, we also observe cylinders below $T^*_{ODT} = 8.0$, but only down to $T^* = 4.5$, below which we observe spatially ordered spheres (Figure 6). Therefore, this temperature, $T^* = 4.5$, can be be declared as an order–order transition (OOT) temperature. The same OOT temperature is found for all box sizes considered. At low volume fractions, $\Phi = 0.4$, 0.3, and 0.2, we can see spatially ordered spheres below the ODT temperatures, $T^*_{ODT} = 7.5$, 7.0, and 6.5, respectively, for all box sizes. This order is probably augmented by the periodic boundary conditions of the cubic simulation box. At $\Phi = 0.1$, however, the spheres (micelles) are observed below $T^* = 6.0$, but their spatial arrangement is disordered, which suggests that this temperature corresponds to critical micelle temperature, $T_{CMT}$, rather than order–disorder transition temperature, $T_{ODT}$. It is well-known that the simulation of micelle formation is difficult,[20] and we have to approach the data for relatively small simulation boxes, such as ours, with considerable caution.

Now, it is interesting to compare the above phase diagram with experimental phase diagram by Lodge and co-workers, shown in Figure 2, who investigated the phase behavior of block copolymer solutions of varying selectivity. Since our solvent is perfectly selective, we compare our phase diagram with the phase diagram for poly(styrene-*b*-isoprene) (SI) with similar

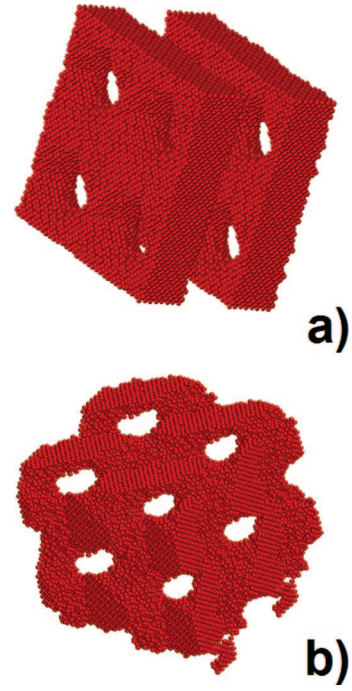


**Figure 5.** Snapshots of perforated lamellar phase at $\Phi = 0.7$; only B-blocks are shown: (a) the $32 \times 32 \times 32$ box at $T^* = 2.0$; (b) the $64 \times 32 \times 32$ box at $T^* = 5.0$.

blocks (15–13) mixed with the most selective solvent considered, i.e., DMP. The experimental phase diagram, shown in Figure 2, exhibits the following sequence of phases upon addition of DMP: layers, gyroid phase, cylinders, and spheres.

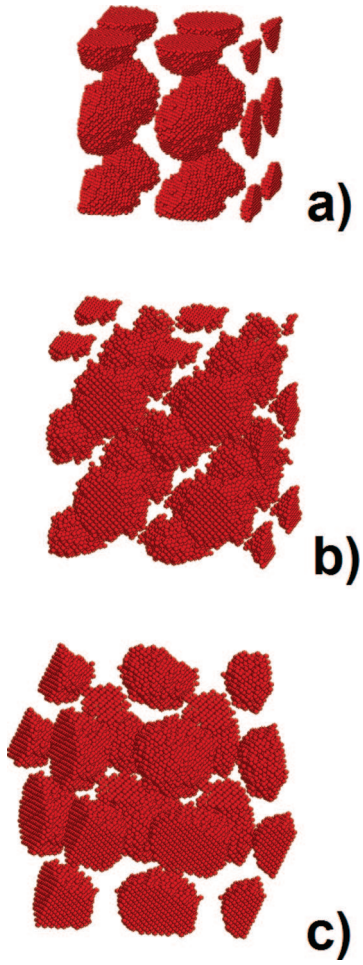


**Figure 6.** Snapshots of spherical phase at $\Phi = 0.5$; only B-blocks are shown: (a) the $32 \times 32 \times 32$ box at $T^* = 1.9$; (b) the $64 \times 32 \times 32$ box at $T^* = 4.5$; (c) the $64 \times 64 \times 64$ box at $T^* = 2.5$.

We also notice that the solvent tends to dissolve the microphase, which means that the ODT temperature decreases as the solvent is added. Furthermore, at low temperatures (below 150 °C) and low volume fractions (roughly below 0.2) spatially disordered micelles can be found.

If we were to consider the PL phase as a metastable phase, covering the G phase, and the B phase as corresponding to the G phase, then the sequence of phases upon solvent addition would be the same for both phase diagrams. There are also other features which indicate a qualitative resemblance of both diagrams. For example, the shape of the ODT line is similar, first decreasing with decreasing copolymer volume fraction to about $\Phi = 0.7$ and reaching a plateau from about $\Phi = 0.7$ to about $\Phi = 0.3$. Also, the location and shapes of the OOT lines are similar, with layers stable above approximately $\Phi = 0.75$ and with spheres stable approximately below $\Phi = 0.5$ for simulation and below $\Phi = 0.4$ for experiment. We also observe B and PL phases at $\Phi = 0.7$, close to the volume fractions at which Lodge and co-workers found a G phase. At lower temperatures, however, they did not find a gyroid phase from their experiments, but we find either B or PL phases at all temperatures for $\Phi = 0.7$ volume fraction. The problem of stability and an exact location of the gyroid phase remains a challenge. For pure diblock melts, most experimental and theoretical studies conclude that the gyroid phase is stable only in the vicinity of the ODT temperature. Recently, however, Fredrickson and co-workers[19] found that the gyroid phase is stable in a narrow composition range for all temperatures below the ODT temperature.

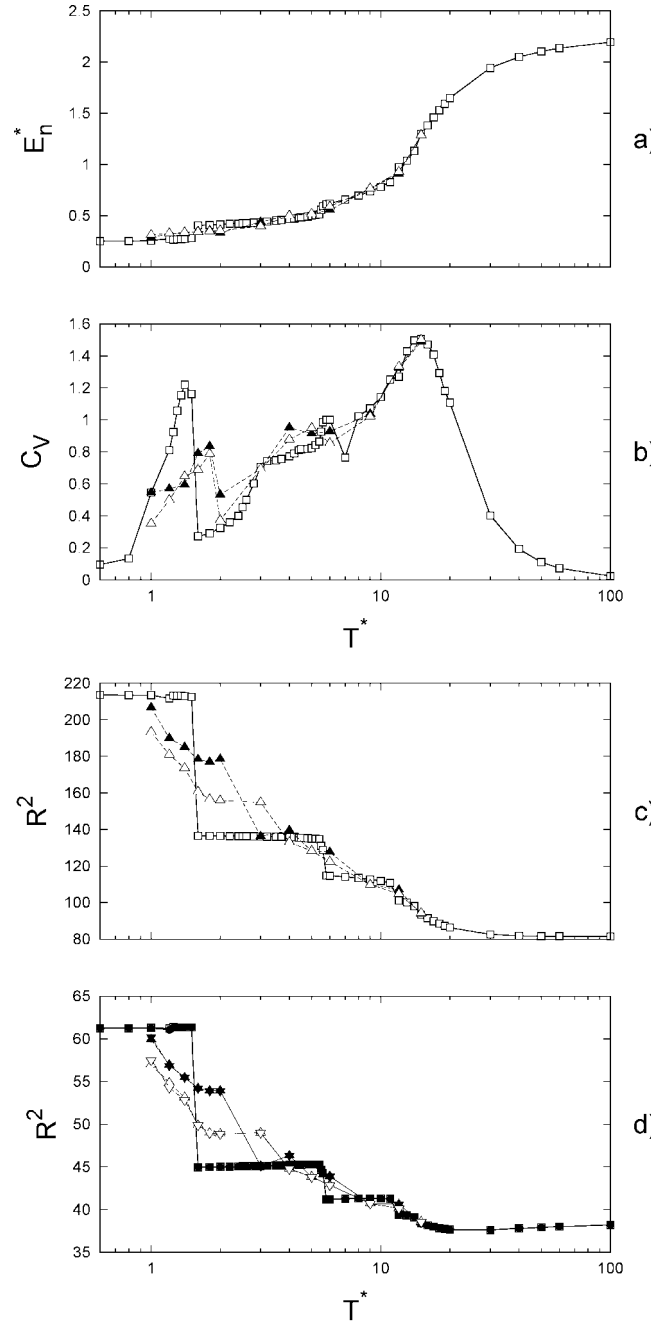


**Figure 7.** Temperature dependencies of selected properties for $\Phi = 1.0$ (□, the $32 \times 32 \times 32$ box; ▲, the $64 \times 32 \times 32$ box; △, the $64 \times 64 \times 64$ box): (a) energy per lattice site, $E^*/n_a$; (b) specific heat, $C_v$; (c) mean-squared end-to-end distance for the whole diblock chain, $R^2$; (d) mean-squared end-to-end distances for the A-blocks (□, ▲, and △ denote the same as above) and the B-blocks (●, the $32 \times 32 \times 32$ box; ▼, the $64 \times 32 \times 32$ box; ▽, the $64 \times 64 \times 64$ box). Both quantities are equal due to symmetry with respect to A and B for the melt.

For selected volume fraction, $\Phi = 1.0$, 0.7, and 0.5, the total energy per lattice site, $E^*/n_a$, the specific heat, $C_v$, the mean-squared end-to-end distance for the whole diblock chain, $R^2$, and the mean-squared end-to-end distances for individual blocks are presented in Figures 7–9 for different box sizes. As expected, the size effects are more pronounced at low temperatures because it is increasingly difficult to fit well-formed nanostructures into the simulation box; the smaller the box, the more difficult it is. The other reason for such effects is an increase of uncontrollable relaxations times at low $T^*$. However, above $T^* = 2.0$ (below the ODT line) the data do not significantly depend

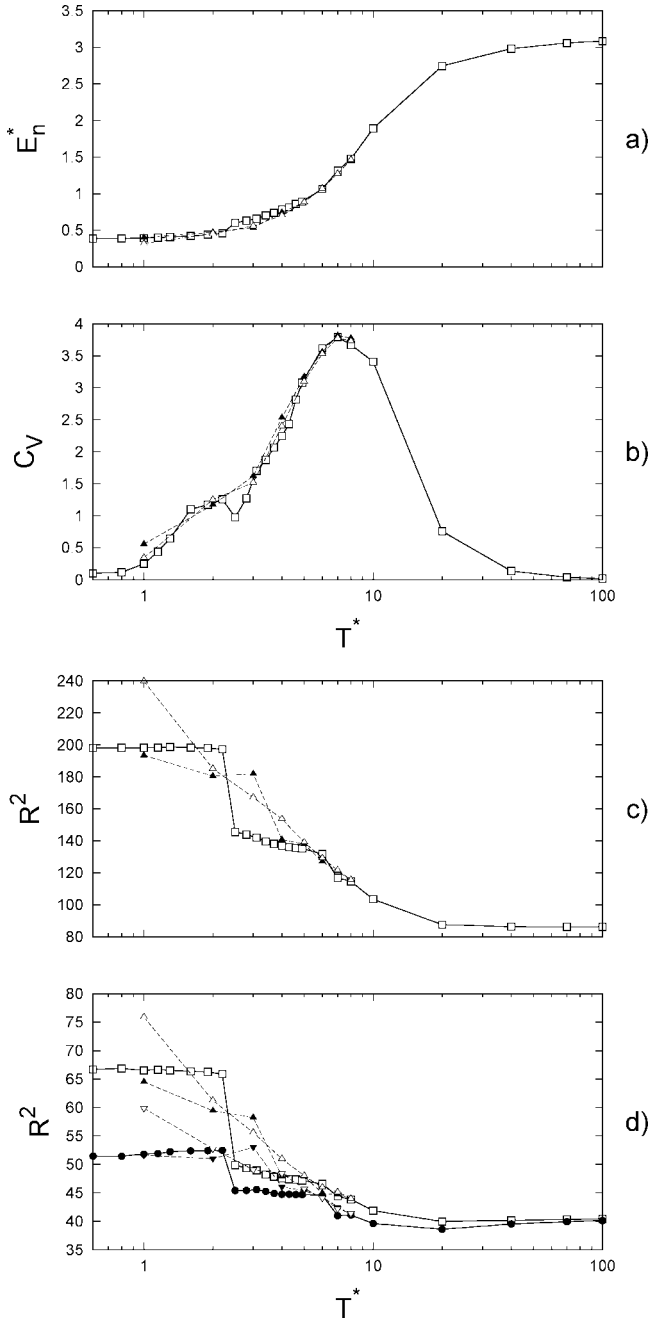


**Figure 8.** Temperature dependencies of selected properties for $\Phi = 0.7$ (□, the 32 × 32 × 32 box; ▲, the 64 × 32 × 32 box; △, the 64 × 64 × 64 box): (a) energy per lattice site, $E^*/n_a$; (b) specific heat, $C_v$; (c) mean-squared end-to-end distance for the whole diblock chain, $R^2$; (d) mean-squared end-to-end distances for the A-blocks (□, ▲, and △ denote the same as above) and the B-blocks (●, the 32 × 32 × 32 box; ▼, the 64 × 32 × 32 box; ▽, the 64 × 64 × 64 box).

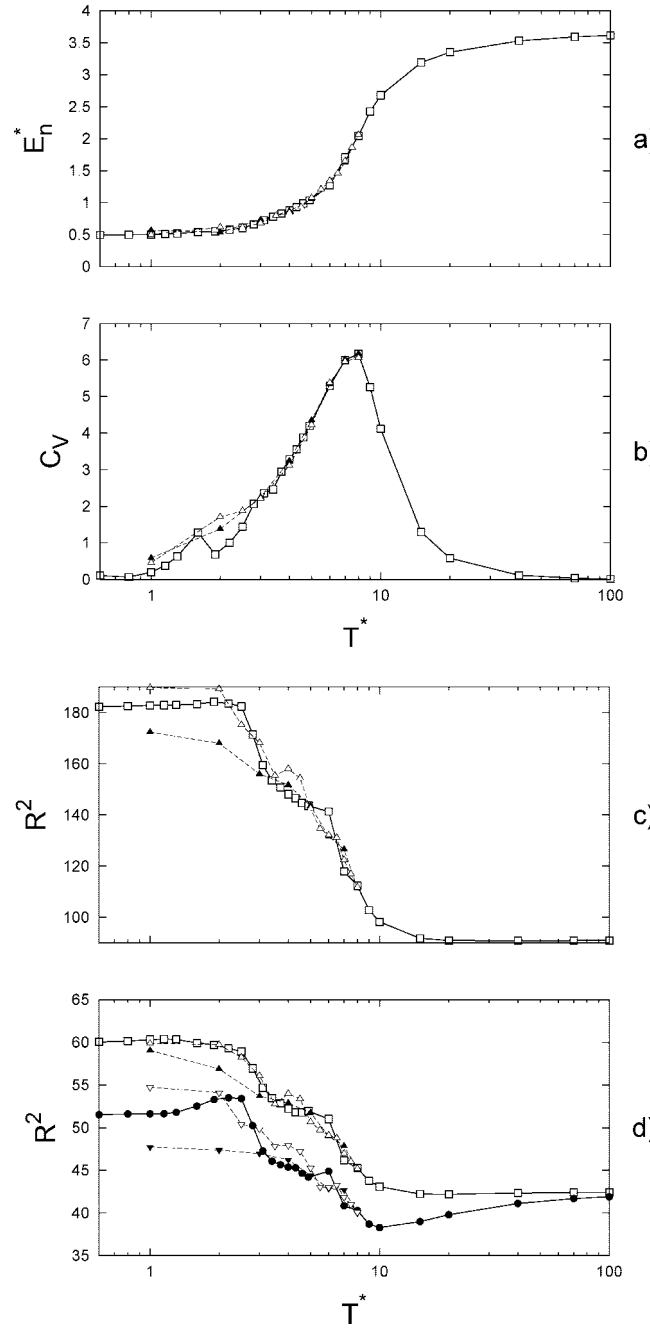


**Figure 9.** Temperature dependencies of selected properties for $\Phi = 0.5$ (□, the 32 × 32 × 32 box; ▲, the 64 × 32 × 32 box; Δ, the 64 × 64 × 64 box): (a) energy per lattice site, $E^*/n_a$; (b) specific heat, $C_v$; (c) mean-squared end-to-end distance for the whole diblock chain, $R^2$; (d) mean-squared end-to-end distances for the A-blocks (□, ▲, and △ denote the same as above) and the B-blocks (●, the 32 × 32 × 32 box; ▼, the 64 × 32 × 32 box; ▽, the 64 × 64 × 64 box).

on the box size. For all volume fractions, energy decreases with decreasing temperature, which is consistent with a higher degree of segregation between distinct segments (A and B). The abrupt energy changes as a function of temperature usually correspond to some structural changes of the system. (They can also correspond to finite-size frustrations related to the incommensurateness of the nanostructure periodicity and the box size.) The specific heat, $C_v$, presented in part b the same figures (Figures 7b−9b), exhibits a more complex behavior. At high $T^*$, $C_v$ is small, and it increases upon cooling, reaching a maximum (both local and global) at a temperature, which we identify as the ODT temperature for volume fractions from 1.0 to 0.2 and at some ordering temperature for $\Phi = 0.1$, which may be the critical micelle temperature (CMT). The above identifications are based on examination of numerous MC configurations and also on the structural behavior of individual chains and blocks, shown in panels c and d of Figures 7–9. The ODT temperatures can also be inferred from the copolymer chain expansion and the individual blocks expansion, upon cooling, as presented in panels c and d.

Let us examine more closely the strong segregation regime below $T^* = 2.0$. At high volume fraction, one observes a secondary maximum in the specific heat accompanied by a significant increase of the chain size upon cooling. What is perhaps even more intriguing is the smoothing of the interfaces separating A-rich and B-rich microdomains upon cooling, as

shown in Figure 3 for all box sizes; at lower $T^*$'s (Figure 3a,c,e) the interface is smooth, in contrast to higher $T^*$'s (Figure 3b,d,f). Figure 7b also suggests that the position and the height of the low-$T^*$ peaks depend significantly on the box size, which may indicate a finite-size effect of the lattice model, as does $R^2$ (Figure 7a,b) at very low $T^*$. We reported a similar behavior for the diblock and triblock melts previously.[17,21] While it was not clear if such behavior was due to a interfacial low-temperature effect or if it was an artifact of the underlying lattice, we conjectured a glass transition. Either way, this calls for off-lattice simulations but does not impact the general phase diagrams and the main conclusion.

## IV. Conclusion

Using a lattice Monte Carlo method, we investigate 16−16 symmetric diblock in selective solvent in boxes of various sizes. We report temperature dependencies for a number of quantities such as energy, specific heat, and mean-squared end-to-end distances. We construct a phase diagram, using the thermodynamic and structural quantities, as well as selected snapshots from the Monte Carlo configurations. The simulated phase diagram is compared with the experimental data, obtained by Lodge and co-workers,[8] for poly(styrene-*b*-isoprene) (SI) with similar blocks (15−13) mixed with DMP. We find a qualitative resemblance of both diagrams. In particular, if were were to treat the B and PL phases as covering the G phase, the sequence of phases upon solvent addition would be the same, and also the topology and geometry would be similar for both phase diagrams. The problems of micelle formation at low concentrations, the macrophase separation, and the phase behavior at low temperatures (very strong segregation) remain open for further studies. We also intend to focus on bicontinuous cubic phase near $\Phi = 0.7$.

**Acknowledgment.** M.B. thanks M. W. Matsen for helpful comments. M.R. acknowledges an NSF Grant (CTS-0625341).

## References and Notes

(1) de Gennes, P. G. *Scaling Concepts in Polymer Physics*; Cornell University Press: Ithaca, NY, 1979.
(2) Hamley, I. W. *Developments in Block Copolymer Science and Technology*; John Wiley & Sons: Berlin, 2004.
(3) Hamley, I. W. *Block Copolymers in Solution*; John Wiley & Sons: Berlin, 2005.
(4) Lodge, T. P. *Macromolecules* **2003**, *204*, 265.
(5) Matsen, M. W. *J. Phys.: Condens. Matter* **2002**, *14*, R21.
(6) Khandpur, A. K.; Forster, S.; Bates, F. S.; Hamley, I. W.; Ryan, A. J.; Bras, W.; Almdal, K.; Mortensen, K. *Macromolecules* **1995**, *28*, 8796.
(7) Leibler, L. *Macromolecules* **1980**, *13*, 1602.
(8) Lodge, T. P.; Pudil, B.; Hanley, K. J. *Macromolecules* **2002**, *35*, 4707.
(9) Matsen, M. W. *J. Chem. Phys.* **1995**, *102*, 3884.
(10) Banaszak, M.; Whitmore, M. D. *Macromolecules* **1992**, *25*, 3406.
(11) Micka, U.; Binder, K. *Macromol. Theory Simul.* **1995**, *4*, 419.
(12) Vassiliev, O. N.; Matsen, M. W. *J. Chem. Phys.* **2003**, *118*, 7700.
(13) Matsen, M. W.; Griffiths, M. W.; Wickham, R. A.; Vassiliev, O. N. *J. Chem. Phys.* **2006**, *124*, 024904.
(14) Pakula, T. *Macromolecules* **1987**, *20*, 679.
(15) Pakula, T. In *Simulation Methods for Polymers*; Kotelyanskii, M. J., Thedorou, D. N., Eds.; Marcel-Dekker: New York, 2004; Chapter 5.
(16) Banaszak, M.; Wołoszczuk, S.; Pakula, T.; Jurga, S. *Phys. Rev. E* **2002**, *66*, 031804.
(17) Banaszak, M.; Wołoszczuk, S.; Jurga, S.; Pakula, T. *J. Chem. Phys.* **2003**, *119*, 11451.
(18) Fredrickson, G. H.; Helfand, E. *J. Chem. Phys.* **1987**, *87*, 697.
(19) Cochran, E. W.; Garcia-Cervera, C. J.; Fredrickson, G. H. *Macromolecules* **2006**, *39*, 2449.
(20) Milchev, A.; Bhattacharya, A.; Binder, K. *Macromolecules* **2001**, *34*, 1881.
(21) Woloszczuk, S.; Banaszak, M.; Jurga, S.; Pakula, T.; Radosz, M. *J. Chem. Phys.* **2004**, *121*, 12044.

MA0718346